JOURNAL OF NANO- AND ELECTRONIC PHYSICS
Vol. **14** No 4, 04001(4pp) (2022)

ЖУРНАЛ НАНО- ТА ЕЛЕКТРОННОЇ ФІЗИКИ
Том **14** № 4, 04001(4cc) (2022)

Synthesis and Characterization of Nd^{3+} Doped Mg-Cd Ferrite ($Mg_{0.5}Cd_{0.5}Nd_{0.01}Fe_{1.99}O_4$) Nanoparticles Prepared in the Form of a Thick Film for Gas Sensing Applications

Rakesh M. Shedam[1,*], Priyanka P. Kashid[1], Mahadev R. Shedam[2], Ashok B. Gadkari[3], Pradip D. Kamble[2], Shridhar N. Mathad[1,†]

[1] *Department of Engineering Physics, K.L.E. Institute of Technology, Gokul Road, Hubballi, Karnataka 580027, India*
[2] *The New College, Kolhapur, India*
[3] *Department of Physics, GKG College, Kolhapur, India*

(Received 10 April 2022; revised manuscript received 11 August 2022; published online 25 August 2022)

The oxalate co-precipitation method was used to prepare nanocrystallite ferrites with Nd^{3+} added to the general formula $Mg_{1-x}Cd_xFe_2O_4$ ($x = 0.5$). FTIR, XRD, and SEM were all used to characterize the samples. According to XRD, the structure is cubic spinel with orthoferrite ($NdFeO_3$) as a secondary phase. The crystallite size is 36.79 nm. SEM analysis of surface morphology indicates a grain size of 0.38 μm. There are two strong absorption bands observed in the FTIR spectrum in the range of 350-800 cm^{-1}. We were able to detect various gases such as Cl_2, LPG, and ethanol using the gas sensor from room temperature to 500 °C. For 100 ppm ethanol gas at 500 °C, the $Mg_{0.5}Cd_{0.5}Nd_{0.01}Fe_{1.99}O_4$ composition has the greatest response. Mg-Cd ferrite sensor samples with Nd^{3+} added show good response and recovery time. Material composition, test gas, and grain size determine the time to complete the test.

Keywords: Nanocrystallite, Chemical synthesis, SEM, Selectivity, Response time.

DOI: 10.21272/jnep.14(4).04001 PACS numbers: 68.37.Hk, 81.20.Ka

1. INTRODUCTION

Due to safety concerns and environmental monitoring needs, gas sensors are receiving a lot of attention in today's society. The amount of everyday air pollution has increased dramatically as a result of rising industrialization and automotive production in recent years. Pollutants include gases, volatile organic compounds, suspended particles, and others. As a result, scientists, engineers, and technocrats are working to reduce air pollution at the source by detecting, controlling, and lowering pollutants [1, 2]. Due to its outstanding physical and chemical properties, mechanical properties, magnetism, and dielectric properties, a tertiary mixed metal oxide with cubic spinel structures has been identified as a promising material for electrochemical energy storage, televisions, transformers, magnetic recording media, and biomedical applications [3-8]. Researchers have devised a simple, stable, and successful method for synthesizing nanosized materials that maintains structural characteristics and provides a high specific surface area in the last several years [9, 10]. There are many applications for nanocrystalline magnetic particles, such as ferrofluids, magnetic drug delivery, hyperthermia, etc. [11-14]. Iron and steel ferrites are intrinsically magnetic due to their chemical composition, but their extrinsic magnetic properties are highly dependent on their microstructure [15]. The formula AB_2O_4 represents cubic spinal structures, where "A" is a bivalent metal ion and "B" is a trivalent metal ion. A spinel ferrite crystal structure has 8 tetrahedral (A-sites) and 16 octahedral (B-sites) oxygen ions [16]. As a result, among the interstitials in spinel ferrites, there are a considerable number of unoccupied A and B sites that can be occupied by cations. Zinc ion sites in tetrahedra and iron ions dispersed over the tetrahedral and octahedral characterize the spinel structure of $ZnFe_2O_4$ nanocrystalline semiconductor [17]. The physicochemical, electrical, and magnetic properties of spinel ferrites show a major effect of adding cations and how they are distributed between the tetrahedral and octahedral interstitial sites, as well as influencing the manufacturing procedure to a large extent. These parameters are determined by the synthesis technique, calcining temperature, chemical content, concentration and type of dopants utilized [16, 17]. Microwave applications benefit from their low cost, high saturation magnetization, high Curie temperature, high resistance, and low eddy current losses [18].

The effect of Nd^{3+} ions added to Mg-Cd nanocrystallite ferrites prepared by the oxalate co-precipitation technique on the gas sensing characteristics for LPG, chlorine (Cl_2), and ethanol (C_2H_5OH) was investigated in this paper.

2. EXPERIMENTAL PROCEDURES

Spinel ferrites were synthesized by the oxalate co-precipitation method with 5 wt. % Nd^{3+} ions added and with the general formula $Mg_{1-x}Cd_xFe_2O_4$ ($x = 0.5$). Starting materials included High Purity Analytical Reagents (AR) $MgSO_4.7H_2O$ (purity 99.5 %, Thomas Baker), $3CdSO_4.8H_2O$ (purity 99.99 %, Thomas Baker), $FeSO_4.7H_2O$ (purity 99.5 %) and $Nd_2(SO_4)_3.8H_2O$ (Alfa Aesar).

All the materials were weighed according to their proportions and dissolved in double distilled water. A solution with pH 4.0 can be maintained by adding

* shedam.rakesh@gmail.com
† physicssiddu@kleit.ac.in

 © 2022 Sumy State University

H_2SO_4 concentration. The solution was stirred until complete precipitation was obtained with the addition of ammonium oxalate of AR grade (Sd Fine-Chem. Ltd). In order for the magnesium oxalate, cadmium oxalate, and ferrous oxalate precipitate to settle down, it was heated on a hot plate for 1 h. A quantitative filter paper (HiMedia Lab) was used to filter and wash the precipitate several times with distilled water. A barium chloride test confirmed the removal of sulphate ions. After drying and pre-sintering at 100 °C for 1 h, the precipitate was cooled. An agate mortar was used to mill pre-sintered powders and to sinter them for 5 h at 500 °C.

The sintered powder was mixed with the binder (2 wt. % polyvinyl alcohol). In addition to 90 wt. %, binders such as 4 wt. % ethyl cellulose, 5 wt. % 2-(2-butoxy ethoxy) ethyl acetate, and 1 wt. % ethyl acetate were used. Thick films were created using the screen-printing technique.

The test gases, chlorine, LPG and ethanol were obtained from a commercially available gas cylinder. At room temperature, the Philips PW-3710 X-ray powder diffractometer measured patterns in the range of 200-80 using Cu-K radiation ($\lambda = 1.5424$ Å). Debye Scherrer's formula was used to calculate the crystallite size. A scanning electron microscope (JEOL-JND 6360 model, Japan) was used to examine the surface morphology. Perkin-Elmer FTIR spectrum spectrometer using the pellet technique measured the IR absorption spectra of powdered samples between 350 and 800 cm^{-1}.

3. RESULTS AND DISCUSSION

Structural analysis (XRD, SEM and FTIR) of 5 wt. % Nd^{3+} ions added to the Mg-Cd ferrites under investigation has already been reported [20].

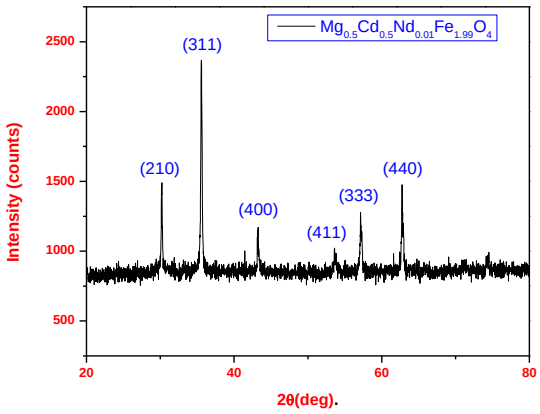

Fig. 1 – XRD pattern of $Mg_{0.5}Cd_{0.5}Nd_{0.01}Fe_{1.99}O_4$ ferrites

The XRD pattern of $Mg_{0.5}Cd_{0.5}Nd_{0.01}Fe_{1.99}O_4$ with Nd^{3+} addition is shown in Fig. 1. In samples containing orthoferrite ($NdFeO_3$) secondary phases, cubic spinel structures can be found, 36.79 nm is the average size of crystallization.

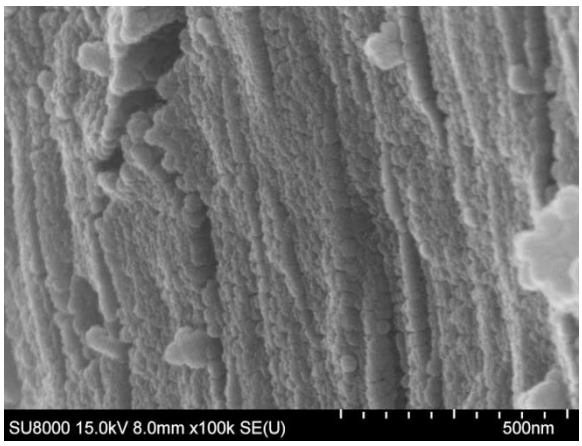

Fig. 2 – SEM image of $Mg_{0.5}Cd_{0.5}Nd_{0.01}Fe_{1.99}O_4$

In Fig. 2, we show a typical SEM micrograph of $Mg_{0.5}Cd_{0.5}Nd_{0.01}Fe_{1.99}O_4$. Using the linear intercept method, Table 1 presents the average grain size of the samples. The range is about 0.38 µm. Based on the table, it can be seen that the grain size of Mg-Cd ferrites with added Nd^{3+} ions is smaller than that of the ferrites without added ions. The addition of Nd^{3+} ions slows down grain growth, probably because it is deposited at the grain boundaries and, therefore, hinders grain motion [19].

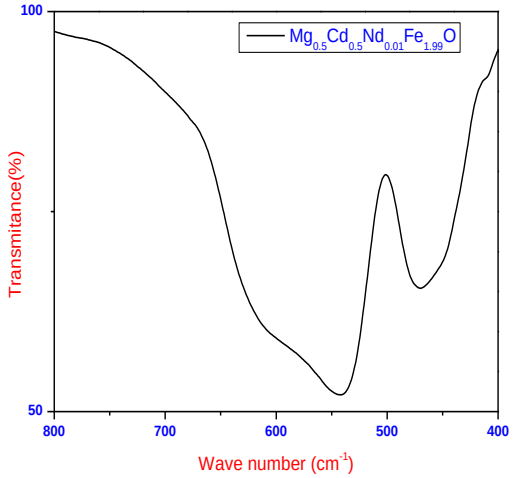

Fig. 3 – Infrared absorption spectra of $Mg_{0.5}Cd_{0.5}Nd_{0.01}Fe_{1.99}O_4$

The FTIR spectrum of $Mg_{0.5}Cd_{0.5}Nd_{0.01}Fe_{1.99}O_4$ is shown in Fig. 3. In the range 543 cm^{-1} and 471 cm^{-1} (ν_1 and ν_2), two absorption bands can be seen. The bands indicate well-formed ferrites [19].

Table 1 – Data on X-ray analysis of the $Mg_{0.5}Cd_{0.5}Nd_{0.01}Fe_{1.99}O_4$ system

Sample	Crystal size *D* (nm)	Lattice constant (Å)	X-ray density	Bond length (Å)		Ionic radii (Å)		Abortion band	
		a		A-O site	B-O site	r_A	r_B	ν_1	ν_2
0.5	36.79	8.9014	4.3189	2.1478	2.2829	0.7979	0.9329	475.51	585.29

3.1 Gas Sensing Property

Ethanol, chlorine, and LPG were chosen to demonstrate the gas sensing performance of Nd^{3+} added Mg-Cd ferrite material particles generated by the co-precipitation process. The working temperature of the sensor corresponds to its reaction to ethanol, chlorine, and LPG gases, as shown in Fig. 4, which were the three gases, to which it showed the greatest selectivity (i.e., the highest response). The gas-sensing performance of thick films with high surface-to-volume ratio sensors and near-spherical mesoporous surface shape was good. The species and amount of oxygen chemisorbed on the surface regulate the resistance of ferrites, which are gas detecting mechanisms [20]. Nd-Mg-Cd ferrite sensors' performance is influenced by oxygen deposited on their surfaces. The surface of the molecular oxygen adsorbent is chemically adsorbent. During the following procedure, the molecular oxygen adsorbent is chemically adsorbed on the surface of a Nd-Mg-Cd sensor:

$$O_{2gas} \leftrightarrow O^-_{2ads} \leftrightarrow 2O^-_{ads} \leftrightarrow O^{2-}_{ads}. \qquad (1)$$

The equilibrium shifts to the right with increasing temperature, resulting in the reduction of conductance. Equilibrium at high temperatures affects conductance and leads to decreasing conductance. The oxygen molecule takes electrons from the Nd-Mg-Cd ferrite sensors, causing them to become more resistant [20]. As a result of their reaction with chemisorbed oxygen, Nd-Mg-Cd sensors are sensitive to reducing gases such as ethanol and LPG, which results in decreased resistance. The overall interaction on the surface of the ferrite sensor with oxygen species O^- and O_2^- is that of reducing gases, as indicated in the diagram [20]:

$$R_{(gas)} \leftrightarrow R_{(ads)}, \qquad (2)$$

$$R_{(ads)} + O^-_{(ads)} \leftrightarrow RO_{(ads)} + e^-. \qquad (3)$$

(i) The ferrite sensor element reacts with chemisorbed oxygen when exposed to LPG. Adsorbed oxygen is removed from LPG when it interacts with hydrocarbons (C_nH_{2n-2}). LPG reacts with chemisorbed oxygen as [22]

$$2C_nH_{2n+2} + O_2^- \rightarrow 2C_nH_{2n}O + 2H_2O + 2e^-, \qquad (4)$$

where C_nH_{2n+2} represents various LPG hydrocarbons.

(ii) Ethanol reacts with oxygen adsorption to produce electrons in the sensor's conduction band, there is less resistance. Some possible reactions can be described as follows [23, 24]:

$$C_2H_5OH + O_{(ads)}^- \rightarrow C_2H_5O_{(ads)}^- + H_2O, \qquad (5)$$

$$C_2H_5O_{(ads)}^- \rightarrow (C_2H_5)\,O + e^-. \qquad (6)$$

(iii) At present, the chemisorption phenomenon is used to model high temperature behavior in oxide sensors. As chlorine reacts with metal oxides upon contact with the sensor element, chlorides are formed. It could sorb surface oxygen vacancies, or it could react with or displace lattice oxygen. The following is a description of Cl_2 chemisorption behavior on sensor surfaces [25]:

$$Cl_2 + 2O^{2-}_{suf} \rightarrow 2Cl^-_{suf} + O_2 + 2e^-, \qquad (7)$$

$$Cl_2 + 2O_0^x \leftrightarrow 2Cl_0^{\bullet} + O_2 + 2e. \qquad (8)$$

Kroger-Vink notation is used only for Eq. (8). A prime represents a negative charge, a dot represents a positive charge, and x represents neutrality, according to the lattice. Atoms with subscripts indicate normal sites of atoms; electrons with n indicate conduction electrons. As a result, surf and o denote species that adsorb on the surface and species that occupy lattice oxygen sites, respectively.

Nd-Mg-Cd sensor resistance decreases due to reactions (7) and (8) that donate electrons to the conduction band.

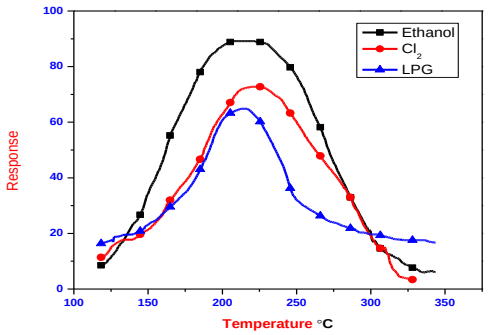

Fig. 4 – Variation of sensitivity as a function of the operating temperature for 5 wt. % Nd^{3+} added $Mg_{0.5}Cd_{0.5}Nd_{0.01}Fe_{1.99}O_4$ system

Nd^{3+} ions added to a $Mg_{1-x}Cd_xFe_2O_4$ ($x = 0.5$) ferrite sensor operate at 215 °C with 91 % sensitivity to C_2H_5OH compared to 64 % for LPG and 72 % for Cl_2. With high sensitivity and selectivity, this sensor detects ethanol. Because of its smaller specific area and lower surface activity, the sensor requires higher operating temperatures, resulting in a weaker interaction between test gases and the sensor [20]. This shows that gas sensitivities are thermally activated and vary depending on the type and composition of the gas.

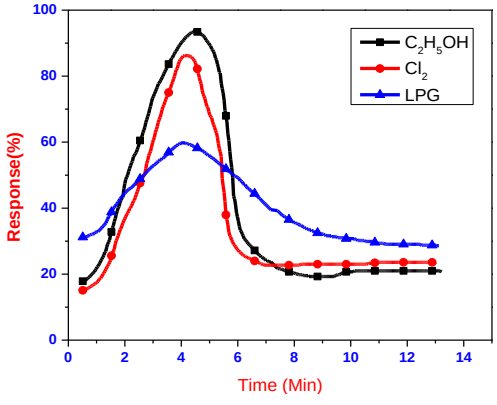

Fig. 5 – Response and recovery characteristic of 5 wt. % Nd^{3+} added $Mg_{0.5}Cd_{0.5}Nd_{0.01}Fe_{1.99}O_4$ system

The response-recovery time of a gas sensor is critical when it is subjected to decreasing gas and subsequently removed. The response-recovery curves of Nd^{3+} ions added to $Mg_{0.5}Cd_{0.5}Nd_{0.01}Fe_{1.99}O_4$ for LPG, Cl_2 and C_2H_5OH are shown in Fig 5. It can be seen from the

figure that, $Mg_{0.5}Cd_{0.5}Nd_{0.01}Fe_{1.99}O_4$ ferrite containing Nd^{3+} ions responds quickly (180 s) to LPG and (240 s) to C_2H_5OH. The sensor element has a large recovery time (~ 360 s).

4. CONCLUSIONS

Mg-Cd ferrites with Nd^{3+} ions added exhibit biphasic nature based on XRD. The average crystallite size is 36.79 nm. SEM grain size shows 0.38 μm, FTIR shows well-formed ferrites. $Mg_{0.5}Cd_{0.5}Nd_{0.01}Fe_{1.99}O_4$ ferrite sensor with Nd^{3+} ions added exhibits higher response than Mg-Cd ferrites. The maximum response was observed on the sensor at 100 ppm. Ethanol is more sensitive, and LPG and chlorine are less sensitive. Microstructure, temperature, gas substitutions and test gas type have a significant impact on gas response.

REFERENCES

1. A. Dey, *Mater. Sci. Eng. B* **229**, 206 (2018).
2. N.S. Ramgir, P.K. Sharma, N. Datta, M. Kaur, A.K. Debnath, D.K. Aswal S.K. Gupta, *Sensor. Actuat. B* **186**, 718 (2013).
3. R.Z. Wang, P. Hong, S. Peng, T. Zou, Y. Yang, X. Xing, Z. Zhao, Z. Yan, Y. Wang, *Electrochim. Acta* **299**, 312 (2019).
4. M. Amiri, M. Salavati-Niasari, A. Akbari, *Adv. Colloid Interface Sci.* **265**, 29 (2019).
5. K.R. Sanadi, S.P. Patil, V.G. Parale, H.H. Park, G.S. Kamble, H.M. Yadav, *J. Mater. Sci.: Mater. Electron.* **29** No 9, 7274 (2018).
6. V.D. Phadtare, V.G. Parale, G.K. Kulkarni, H.H. Park, V.R. Puri, *J. Alloy. Compd.* **765**, 878 (2018).
7. V.D. Phadtare, V.G. Parale, G.K. Kulkarni, H.H. Park, V.R. Puri, *Ceram. Int.* **44** No 7, 7515 (2018).
8. H.S. Jadhav, A. Roy, G.M. Thorat, J.G. Seo, *Inorg. Chem. Front.* **5**, 1115 (2018).
9. V.G. Parale, K.Y. Lee, H.H. Park, *J. Korean Ceram. Soc.* **54** No 3, 184 (2017).
10. A.I. Ivanets, V. Srivastava, M.Yu. Roshchina, M. Sillanpaa, V.G. Prozorovich, V.V. Pankov, *Ceram. Int.* **44** No 8, 9097 (2018).
11. A. Goldman, *Modern Ferrite Technology* (New York: Springer: 2006).
12. B.G. Toksha, E. Sagar, S.M. Patange, K.M. Jadhav, *Solid State Commun.* **147**, 479 (2008).
13. U. Hafeli, W. Schutt, J. Teller, M. Zborowski, *Applications of Magnetic Targeting in Diagnosis and Therapy – Possibility and Limitations: A Mini Review, in Scientific and Clinical Applications of Magnetic Carriers* (New York: Plenum: 1997).
14. S.E. Shirsath, B.G. Toksha, R.H. Kadam, S.M. Patange, D.R. Mane, G.S. Jangam, A. Ghasemi, *J. Phys. Chem. Solids* **71**, 1669 (2010).
15. S.S. Yattinahallia, S.B. Kapatkarb, N.H. Ayachitb, S.N. Mathada, *Int. J. Self-Propag. High Temp. Synth.* **22** No 3, 147 (2013).
16. N. Rezlescu, E. Rezlescu, P.D. Popa, M.L. Craus, L. Rezlescu, *J. Magn. Magn. Mater.* **182**, 199 (1998).
17. M. Wang, M. Yang, X. Zhao, L. Ma, X. Shen, G. Cao, *Sci. China Mater.* **59** No 7, 558 (2016).
18. M.K. Rendale, S.N. Mathad, V. Puri, *Int. J. Self-Propag. High Temp. Synth.* **24** No 2, 78 (2015).
19. A.B. Gadkari, T.J. Shinde, P.N. Vasambekar, *Mater. Charact.* **60** No 11, 1328 (2009).
20. A.B. Gadkari, T.J. Shinde, P.N. Vasambekar, *Sensor. Actuat. B* **178**, 34 (2013).
21. C. Doroftei, E. Rezlescu, L. Rezlescu, P.D. Popa, *J. Opt. Adv. Mater.* **10** No 9, 2390 (2008).
22. S. Sing, B.C. Yadav, R. Prakash, B. Bajaj, J.R. Lee, *Appl. Surf. Sci.* **257**, 10763 (2011).
23. V.D. Kapse, S.A. Ghosh, F.C. Raghuwanshi, S.D. Kapashe, U.S. Khandekar, *Talanta* **78** No 1, 19 (2009).
24. Z. Sun, L. Liu, D. Jia, W. Pan, *Simlpe Sensors and Actuators B: Chemical* **125** No 1, 44 (2007).
25. D.H. Dawson, D.E. Williams, *J. Mater. Chem.* **6**, 409 (1996).

Синтез і характеристики наночастинок фериту Mg-Cd ($Mg_{0.5}Cd_{0.5}Nd_{0.01}Fe_{1.99}O_4$), легованого Nd^{3+}, отриманого у формі товстої плівки для датчиків газу

Rakesh M. Shedam[1], Priyanka P. Kashid[1], Mahadev R. Shedam[2], Ashok B. Gadkari[3], Pradip D. Kamble[2], Shridhar N. Mathad[1]

[1] *Department of Engineering Physics, K.L.E. Institute of Technology, Gokul Road, Hubballi, Karnataka 580027, India*
[2] *The New College, Kolhapur, India*
[3] *Department of Physics, GKG College, Kolhapur, India*

Методом оксалатного співосадження отримано нанокристалітні ферити з додаванням Nd^{3+} до зразка, формула якого $Mg_{1-x}Cd_xFe_2O_4$ ($x = 0.5$). Для характеристики зразків використовували FTIR, XRD та SEM. За даними XRD, структура являє собою кубічну шпінель з ортоферитом ($NdFeO_3$) як вторинною фазою. Розмір кристалітів складає 36,8 нм. SEM аналіз морфології поверхні вказує на розмір зерна 0,38 мкм. У спектрі FTIR спостерігаються дві сильні смуги поглинання в діапазоні 350-800 $см^{-1}$. Нам вдалося виявити різні гази, такі як Cl_2, LPG і етанол, використовуючи газовий датчик від кімнатної температури до 500 °C. Для газоподібного етанолу з 100 ppm при 500 °C склад $Mg_{0.5}Cd_{0.5}Nd_{0.01}Fe_{1.99}O_4$ має найбільший відгук. Зразки феритового датчика Mg-Cd з додаванням Nd^{3+} демонструють гарний відгук та час відновлення. Склад матеріалу, тестовий газ і розмір зерен визначають час для завершення тесту.

Ключові слова: Нанокристаліт, Хімічний синтез, SEM, Селективність, Час відгуку.